

Pacific Meridional Modes without Equatorial Pacific Influence[©]

YU ZHANG,^{a,b,c} SHIYUN YU,^{a,b} DILLON J. AMAYA,^{d,e} YU KOSAKA,^f SARAH M. LARSON,^g XUDONG WANG,^h JUN-CHAO YANG,^{a,b} MALTE F. STUECKER,ⁱ SHANG-PING XIE,^c ARTHUR J. MILLER,^c AND XIAOPEI LIN^{a,b}

^aFrontiers Science Center for Deep Ocean Multispheres and Earth System and Physical Oceanography Laboratory, Ocean University of China, Qingdao, China

^bQingdao National Laboratory for Marine Science and Technology, Qingdao, China

^cScripps Institution of Oceanography, University of California San Diego, La Jolla, California

^dCooperative Institute for Research in Environmental Sciences, University of Colorado Boulder, Boulder, Colorado

^eDepartment of Atmospheric and Oceanic Sciences, University of Colorado Boulder, Boulder, Colorado

^fResearch Center for Advanced Science and Technology, The University of Tokyo, Tokyo, Japan

^gDepartment of Marine, Earth, and Atmospheric Sciences, North Carolina State University, Raleigh, North Carolina

^hCollaborative Innovation Center on Forecast and Evaluation of Meteorological Disaster/KLME/ILCEC, Nanjing University of Information Science and Technology, Nanjing, China

ⁱDepartment of Oceanography and International Pacific Research Center, School of Ocean and Earth Science and Technology, University of Hawai'i at Mānoa, Honolulu, Hawai'i

(Manuscript received 19 July 2020, in final form 25 March 2021)

ABSTRACT: Investigating Pacific meridional modes (PMMs) without the influence of tropical Pacific variability is technically difficult if based on observations or fully coupled model simulations due to their overlapping spatial structures. To confront this issue, the present study investigates both the North PMM (NPMM) and South PMM (SPMM) in terms of their associated atmospheric forcing and response processes based on a mechanically decoupled climate model simulation. In this experiment, the climatological wind stress is prescribed over the tropical Pacific, which effectively removes dynamically coupled tropical Pacific variability (e.g., El Niño–Southern Oscillation). Interannual NPMM in this experiment is forced not only by the North Pacific Oscillation but also by a North Pacific triple (NPT) pattern of atmospheric internal variability, which primarily forces decadal NPMM variability. Interannual and decadal variability of the SPMM is partly forced by the South Pacific Oscillation. In turn, both interannual and decadal NPMM variability can excite atmospheric teleconnections over the Northern Hemisphere extratropics by influencing the meridional displacement of the climatological intertropical convergence zone throughout the whole year. Similarly, both interannual and decadal SPMM variability can also excite atmospheric teleconnections over the Southern Hemisphere extratropics by extending or shrinking the climatological South Pacific convergence zone in all seasons. Our results highlight a new poleward pathway by which both the NPMM and SPMM feed back to the extratropical climate, in addition to the equatorward influence on tropical Pacific variability.

KEYWORDS: Pacific Ocean; Atmosphere-ocean interaction; Coupled models

1. Introduction

Tropical Pacific climate varies on a range of time scales, including interannual [El Niño–Southern Oscillation (ENSO); Timmermann et al. 2018] and decadal [tropical Pacific decadal variability (TPDV); Okumura 2013; Liu and Di Lorenzo 2018] time scales. The predictability of ENSO and TPDV is limited by several factors, such as atmospheric high-frequency noise arising from wind bursts (Fedorov et al. 2003; Hu et al. 2014) and the Madden-Julian oscillation (Slingo et al. 1999), systematic model errors in the mean state of the tropical Pacific (Bellenger et al. 2014), and the growth of initial condition perturbations in coupled models (e.g., Larson and Kirtman 2015) due to imperfect observations (McPhaden 2003). Predictability of tropical Pacific climate variations is also thought to be influenced by physical processes originating from the extratropics (Pegion et al. 2020). For

example, stochastic atmospheric forcing in the North Pacific can generate sea surface temperature (SST) variability in the subtropical eastern Pacific related to the so-called Pacific meridional mode (PMM; Chiang and Vimont 2004; Amaya 2019) through the “seasonal footprinting mechanism” (Vimont et al. 2003), which has been shown to impact ENSO (Chang et al. 2007; Larson and Kirtman 2014; Thomas and Vimont 2016; Ma et al. 2017; Amaya et al. 2019). Thus, improving our understanding of PMM-related teleconnections can benefit tropical Pacific climate prediction.

Previous studies suggest that the PMM exists both in the subtropical northeastern [i.e., the North Pacific meridional mode (NPMM); Chiang and Vimont 2004; Di Lorenzo et al. 2015] and southeastern Pacific [i.e., the South Pacific meridional mode (SPMM); Zhang et al. 2014]. The NPMM is thought to be primarily initiated by the southern lobe of the North Pacific Oscillation (NPO; Rogers 1981; Chiang and Vimont 2004), which represents the second mode of sea level pressure (SLP) variability over the North Pacific during boreal winter. By extending as far south as the Hawaiian Islands, the NPO modulates the strength of trade winds, resulting in changes in surface latent heat flux and underlying SST variations to generate the NPMM. The NPO is partly a stochastic atmospheric phenomenon and partly forced by tropical SST

[©] Supplemental information related to this paper is available at the Journals Online website: <https://doi.org/10.1175/JCLI-D-20-0573.s1>.

Corresponding author: Shiyun Yu, yushiyun1177@stu.ouc.edu.cn

anomalies (Stuecker 2018). The NPO-associated SST anomalies can persist into late summer and fall through wind–evaporation–SST (WES) feedback (Xie and Philander 1994; Wu et al. 2010) as well as through shortwave–SST positive feedback (Vimont et al. 2009). In late summer, the intertropical convergence zone (ITCZ) is at its northernmost point and is sensitive to NPMM-related subtropical SST anomalies. As a result, the NPMM can shift the ITCZ meridionally, driving a broad atmospheric circulation response that occupies much of the midlatitude North Pacific basin. This atmospheric response was recently termed the summer deep convection (SDC) response (Amaya et al. 2019; Amaya 2019).

In the southeast Pacific, the SPMM resembles the NPMM, driven stochastically by the northern lobe of the South Pacific Oscillation (SPO; You and Furtado 2017, 2018), a mirror of the NPO over the South Pacific. Although the origins of both NPMM and SPMM are similar, their impacts on the tropical Pacific variability may be time-scale dependent. For instance, some studies suggested that the NPMM primarily impacts ENSO variability (Chang et al. 2007; Larson and Kirtman 2013; Ma et al. 2017; Amaya 2019), while the SPMM is more effective at lower frequencies relevant for TPDV (Okumura 2013; Zhang et al. 2014). In particular, Liguori and Di Lorenzo (2019) used a coupled model in which they artificially suppressed NPMM and SPMM variability. They found that when the NPMM was suppressed, ENSO variability dropped by $\sim 35\%$, while suppressing the SPMM had little impact on ENSO. However, suppressing the NPMM did not have a significant influence on low-frequency variability, but suppressing the SPMM reduced TPDV by $\sim 30\%$.

In contrast, other studies have suggested that the relative influences of the NPMM and SPMM on ENSO and TPDV are of equal importance (Min et al. 2017; Zhao and Di Lorenzo 2020). For example, Lu et al. (2017) showed that externally forced ENSO variability is contributed roughly equally and independently by the Southern and Northern Hemisphere extratropical atmosphere. The debate on the relative contribution to ENSO and TPDV might be related to the different time scales of PMM variability. Indeed, observations and modeling studies have suggested that both NPMM and SPMM are “reddened” as they integrate stochastic atmospheric forcing, suggesting that they include variability both on interannual and decadal time scales (Min et al. 2017; You and Furtado 2018; Stuecker 2018). However, there has been little effort to separate and investigate PMM variability on these two time scales, as almost all related studies have been based on raw (i.e., unfiltered) PMM variations (Stuecker 2018, Amaya 2019).

Separating raw PMM variability “dynamically” into interannual and decadal components, however, is technically not easy if based on observations or fully coupled model simulations. This is due partly to the nature of two-way interaction between the PMM and tropical Pacific variability (Stuecker 2018; You and Furtado 2018; Joh and Di Lorenzo 2019). To remove the effect of tropical Pacific forcing, statistical methods such as linear regression are often employed (Chiang and Vimont 2004; Chang et al. 2007; Min et al. 2017; You and Furtado 2018). However, this approach cannot completely remove ENSO variability because of ENSO’s strong seasonality (Rasmusson and Carpenter 1982) and nonlinearity (An and Jin 2004; Stuecker 2018). Likewise, isolating TPDV is also difficult due to ocean reemergence processes in the extratropics, which can persist SST anomalies from one year to another (Alexander et al. 1999).

In the present study, we address these issues by isolating essential physical processes that force and develop PMM variability by suppressing equatorial Pacific variability using a mechanically decoupled model experiment in which the climatological wind stress is prescribed over the tropical Pacific. Because this simulation effectively removes both ENSO variability and TPDV (Larson et al. 2018a,b), it offers a unique opportunity to investigate PMM dynamics, independent of tropical Pacific forcing. We focus on the forcing and response of atmospheric variability associated with both NPMM and SPMM. We find that interannual NPMM is forced not only by NPO variability but also by a North Pacific tripole variability, which primarily drives decadal NPMM variability. In addition to the atmospheric forcing, NPMM variability can excite atmospheric teleconnections over the Northern Hemisphere extratropics by influencing the meridional migration of climatological ITCZ. For the SPMM, it is found to be partly forced by SPO variability and can also excite atmospheric teleconnections over the Southern Hemisphere extratropics through the extension or contraction of climatological South Pacific convergence zone (SPCZ). While the extratropical-to-tropical link between the PMM and the tropical Pacific has been established, our study identifies a new pathway by which the PMM ultimately feeds back to the extratropical climate.

The rest of the paper is organized as follows. Section 2 introduces the mechanically decoupled experiment, as well as the observational data and methods used in this study. Section 3 investigates the raw PMMs by comparing the model experiment with observations. In section 4, we study the interannual and decadal NPMM variability, in terms of their related atmospheric forcing and response processes. Section 5 investigates the interannual and decadal SPMM variability. Section 6 is a summary with discussion.

2. Data and methods

a. Model experiments

We conduct a mechanically decoupled experiment, referred to as Clim- τ , based on the Geophysical Fluid Dynamic Laboratory coupled model version 2.1 (CM2.1; Delworth et al. 2006). In the Clim- τ , daily climatological wind stress, obtained from a 1000-yr CM2.1 preindustrial control simulation, is prescribed over the tropical Pacific (15°S – 15°N ; dark blue region in Fig. 1) with 10° buffer zone north and south (light blue regions in Fig. 1) where the simulated and prescribed wind stresses are blended, with the weight linearly tapering off. Outside the tropical Pacific, the ocean and atmosphere are fully coupled and free to evolve. To suppress tiny day-to-day fluctuations that remain in the 1000-yr climatology, the prescribed wind stress has been weakly smoothed temporally by removing the annual harmonics higher than 18 (corresponding to a frequency of about 20 days). The model horizontal resolution is 2.5° longitude $\times 2^{\circ}$ latitude for the atmosphere and 1° longitude $\times 1^{\circ}$ latitude for the ocean, with the ocean latitudinal resolution equatorward of 30° getting gradually finer to $1/3^{\circ}$ at the equator. The model is integrated for 310 years, and only the last 300 years are analyzed. Results are consistent when we repeat this Clim- τ experiment using the Community Earth System Model version 1.2 (CESM1 Clim- τ ; Hurrell et al. 2013).

Mechanically decoupling the ocean and atmosphere removes the possibility for anomalous wind-driven ocean

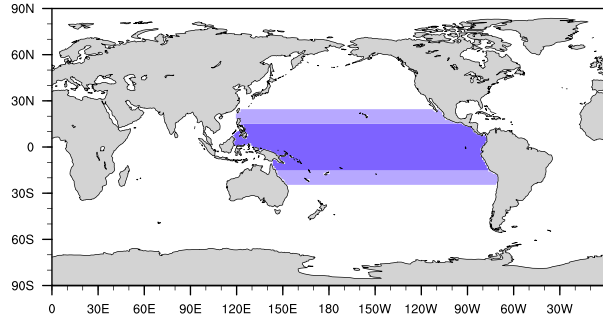


FIG. 1. Schematic of the Clim- τ experiment. Dark blue shading indicates the region where daily climatological wind stress is prescribed (15°S – 15°N). Light blue shading denotes the buffer zones to the north (15° – 25°N) and south (25° – 15°S). Otherwise, the ocean and atmosphere are fully coupled and free to evolve.

dynamics [see Larson et al. (2018b) for impacts on global SST variability]. Specific to ENSO, applying such decoupling in the tropical Pacific eliminates anomalous wind-driven equatorially trapped oceanic Kelvin and Rossby waves that play important roles for ENSO growth and phase transition (Bjerknes 1969; Wyrtki 1975; Zebiak and Cane 1987; McGregor et al. 2012; Larson and Kirtman 2015; Timmermann et al. 2018). As a result, this experiment effectively eliminates ENSO variability in the model at time scales shorter than 10 years (Fig. 2a). This is apparent from the markedly reduced standard deviation of interannual SST (91%) and precipitation (95%) variability over the Niño-3.4 region (5°S – 5°N , 170° – 120°W), compared with a 300-yr

fully coupled CM2.1 control simulation (Fig. 2c). The control (CTRL) simulation is also used to compare the raw PMM simulation with observations. Note that the NCAR CESM1 model shows a similar roughly 90% decline in eastern equatorial Pacific SST variability when the mechanical coupling is disengaged (Larson et al. 2018b).

Additionally, TPDV (at time scales greater than 10 years) is also damped markedly in the Clim- τ (cf. Figs. 2b and 2d). This result contrasts with those from slab-ocean models, which suggest that thermodynamic coupling alone can drive TPDV (Okumura 2013; Zhang et al. 2014). The damped TPDV in the Clim- τ may be due to the damping effect generated by climatological upwelling in the central-eastern equatorial Pacific, which is driven by the climatological trade winds over the tropical Pacific. In the Clim- τ , subsurface temperature anomalies in the central-eastern equatorial Pacific are rather weak since they are mostly induced by the anomalous ocean dynamics, which is largely suppressed due to the model design. SST variability in the Clim- τ , however, can be driven by the air-sea thermodynamic coupling process, as in slab-ocean models. As a result, the climatological upwelling in the central-eastern equatorial Pacific plays a role in damping TPDV. With ENSO variability and TPDV effectively removed from the model, the Clim- τ experiment cuts off the pathway for the equatorial Pacific to influence the midlatitudes. Therefore, our experiment can be used to investigate “pure” PMM variability, without equatorial Pacific influence.

We emphasize that air-sea thermodynamically coupled processes, such as the WES feedback, are still retained. Thus,

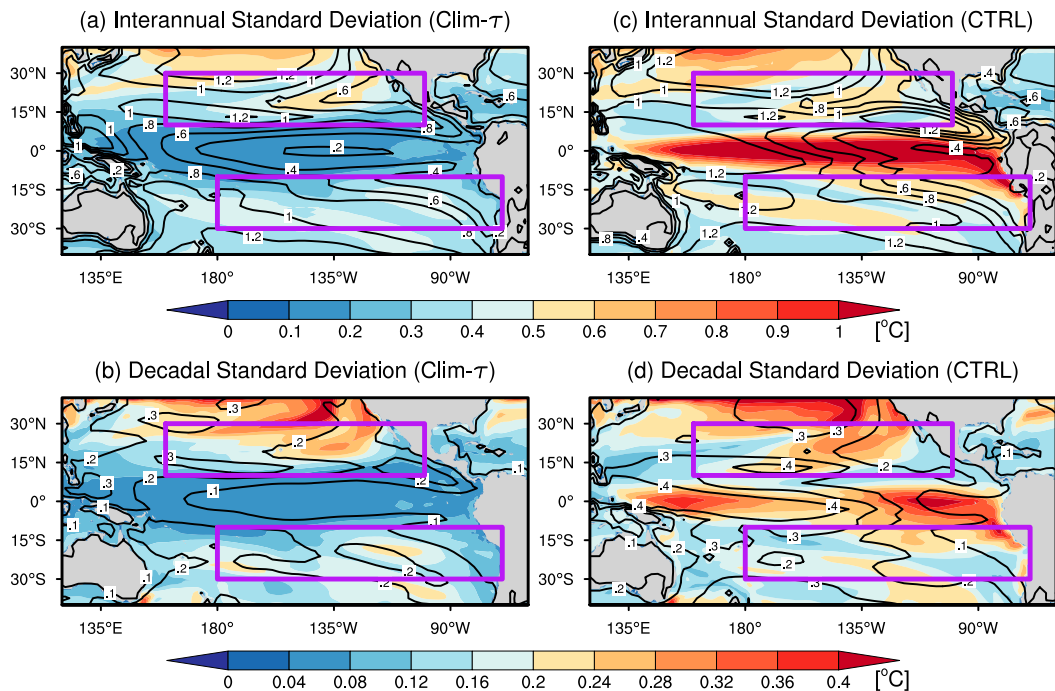


FIG. 2. Standard deviations of (a),(c) interannual and (b),(d) decadal SST (shading: $^{\circ}\text{C}$) and surface zonal wind (black contours; m s^{-1}) anomalies in the (a),(b) Clim- τ and (c),(d) CTRL experiments. Purple boxes denote SVD domains for the NPMM (10° – 30°N , 160°E – 100°W) and SPMM (30° – 10°S , 180° – 70°W), respectively.

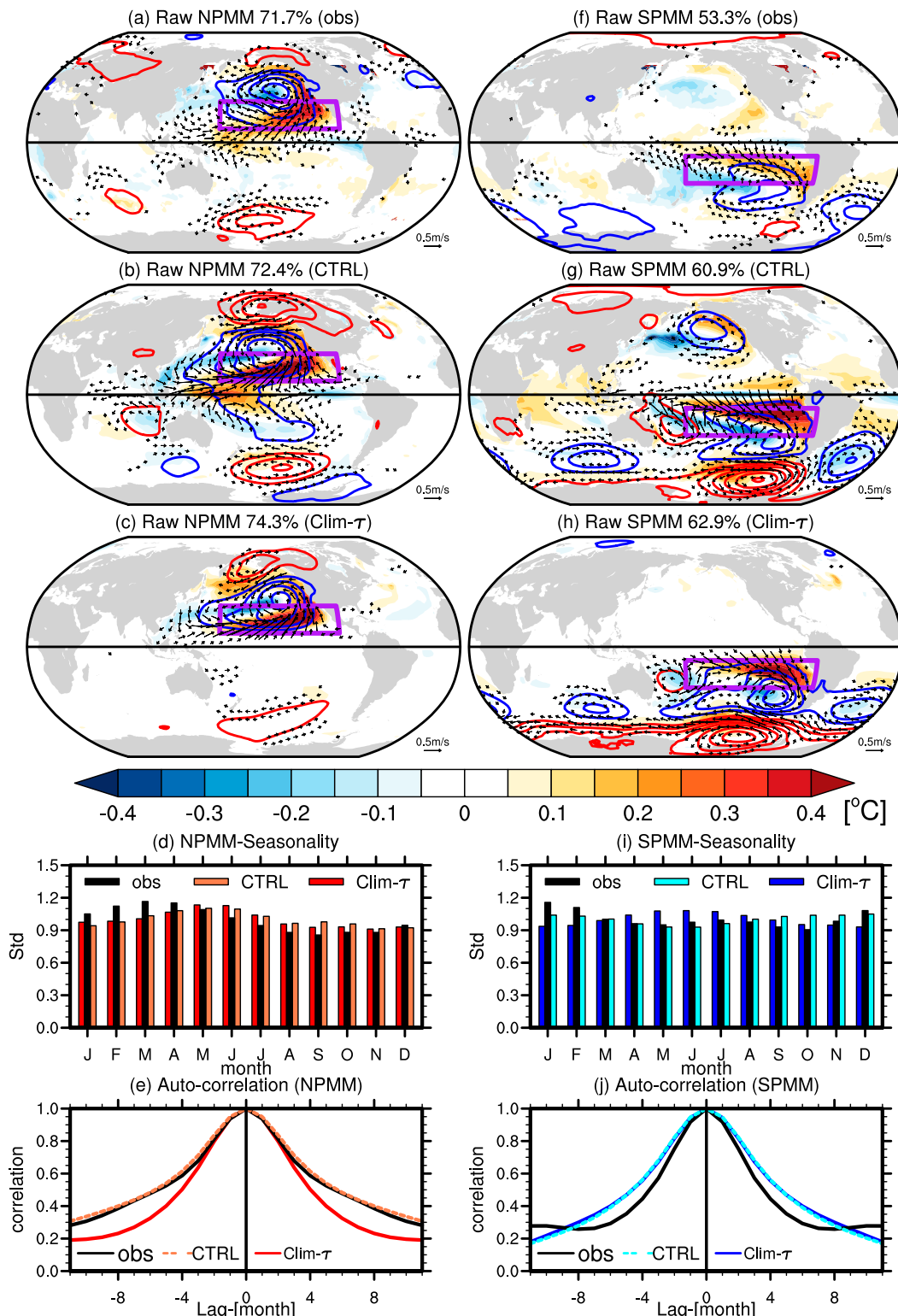


FIG. 3. NPMM and SPMM (unfiltered). Regression maps of SST (shading; $^{\circ}$ C), SLP [contour interval: 0.2 hPa; solid red (blue) is positive (negative) anomaly; zero contour is omitted], and surface wind (arrows; $m s^{-1}$) anomalies against normalized SST EC of the raw PMMs. Shown are (a)–(c) the raw NPMM in observations, CTRL, and Clim- τ , respectively, and (f)–(h) the raw SPMM in observations, CTRL, and Clim- τ , respectively. Small wind speed is omitted for clarity. The horizontal black line denotes the equator. The explained squared covariance fraction of SVD analysis is marked in each panel. Also shown are the monthly standard deviation of the normalized SST EC of the raw (d) NPMM and (i) SPMM, and the autocorrelation of the normalized SST EC of raw (e) NPMM and (j) SPMM.

both the NPMM and SPMM are expected to be simulated. Indeed, the interannual (Fig. 2a) and decadal (Fig. 2b) variability in the Clim- τ experiment both exhibit off-equatorial Pacific SST signatures. In particular, Clim- τ reproduces over 75% of the SST standard deviation (averaged over the purple boxes of Fig. 2) from the CTRL simulation, suggesting that the NPMM and SPMM are largely unaffected by the mechanical decoupling. Moreover, their simulations in the Clim- τ are not likely affected by the meridional width of the restoring domain in which only anomalous ocean dynamics is suppressed. Nevertheless, more research is needed to test the sensitivity of the results shown in this study to the wind-stress-restoring region.

Interestingly, the NPMM- and SPMM-related SSTs in the Clim- τ do not seem to strongly project onto the equator (Figs. 2a,b), which we might have expected from numerous studies using slab-ocean and fully coupled models and observations (Chiang and Vimont 2004; Okumura 2013; Zhang et al. 2014; Di Lorenzo et al. 2015; Min et al. 2017). This weak projection in the Clim- τ may be due largely to the poleward mean Ekman transport, which acts against the equatorward propagation of the PMM variability. Detailed analyses of the role of ocean dynamics in the PMM propagation will be carried out in future research. It is also worth noting that the damped interannual and decadal SST anomalies along the equatorial Pacific can also damp zonal wind and surface wind speed over most of the tropical Pacific (Figs. 2a,b).

We also conduct two atmosphere-only experiments to investigate the atmospheric response to the NPMM (hereafter NPMM experiment) and SPMM (hereafter SPMM experiment) variability, respectively. The two experiments are based on the atmosphere module of CM2.1, and are forced by the SST anomalies only in the respective PMM domain (purple box in Fig. 2 with 10° linear buffer zone outside the box) with climatological SST and sea ice variations globally, all of which are from the Clim- τ experiment. Each experiment is run once, and the length is 300 years, identical to the Clim- τ experiment.

b. Observational data

We also employ observational data to compare with the model simulation. We use SST data from the Hadley Centre Global Sea Ice and Sea Surface Temperature version 1.1 (HadISST v1.1; Rayner et al. 2003). The horizontal resolution is 1° longitude \times 1° latitude. We also use SLP and 10-m surface wind from the European Centre for Medium-Range Weather Forecasts twentieth-century reanalysis (ERA-20C; Poli et al. 2016). The horizontal resolution is 0.75° longitude \times 0.75° latitude. All the data are monthly mean, and the period is from 1900 to 2010. Analyses based on the period after 1950 are similar (not shown).

c. Methods

All the variables from observations and model experiments are linearly detrended after removing the annual cycle. To separate the monthly anomalies into interannual and decadal variability, respectively, we filter the data using a 10-yr high-pass and 10-yr low-pass Lanczos filter. We then perform a singular value decomposition (SVD) analysis between SST and surface wind anomalies to extract the PMM variability for the respective time

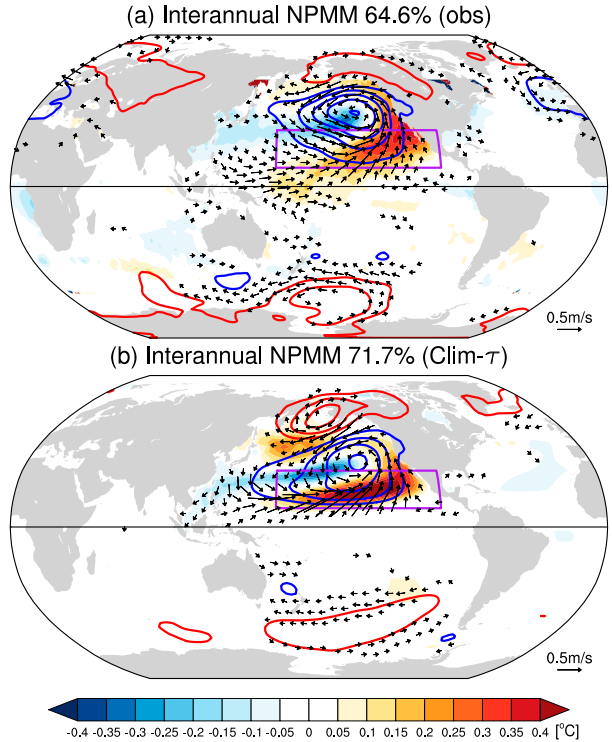


FIG. 4. As in Figs. 3a and 3c, but for interannual NPMM.

scales. We define the raw PMM as the leading SVD mode based on monthly anomalies (i.e., unfiltered), and we define the interannual and decadal PMM as the leading SVD mode of interannual and decadal anomalies, respectively. The SVD analysis is performed over the subtropical northeastern Pacific for the NPMM and southeastern Pacific for the SPMM (purple boxes in Fig. 2), respectively.

In observations and in our CTRL simulation, anomalies associated with tropical Pacific variability are removed before the SVD analysis. Following Chiang and Vimont (2004), we use the cold tongue index (CTI; SST anomalies averaged over 6°S–6°N, 180°–90°W) to represent the tropical Pacific variability. To extract the raw and interannual PMM, given the seasonality of the tropical Pacific variability, we linearly regress out the CTI-related SST and surface wind anomalies for individual calendar months. To extract the decadal PMM, we linearly regress out the 10-yr low-pass filtered CTI for the entire time series.

To examine if decadal NPMM and SPMM variability are stochastically forced by the respective dominant atmospheric variability, we construct a first-order autoregressive (AR-1) model (Di Lorenzo et al. 2010) to reconstruct the PMM index and compare its 10-yr low-pass filtered time series with the SST expansion coefficient (EC) of decadal PMM variability. The AR-1 model is formulated as

$$\frac{d\text{PMM}(t)}{dt} = \text{SLP}(t) - \frac{\text{PMM}(t)}{t_e},$$

where $\text{PMM}(t)$ denotes the reconstructed PMM index at month t ; $\text{SLP}(t)$ denotes the normalized principal component

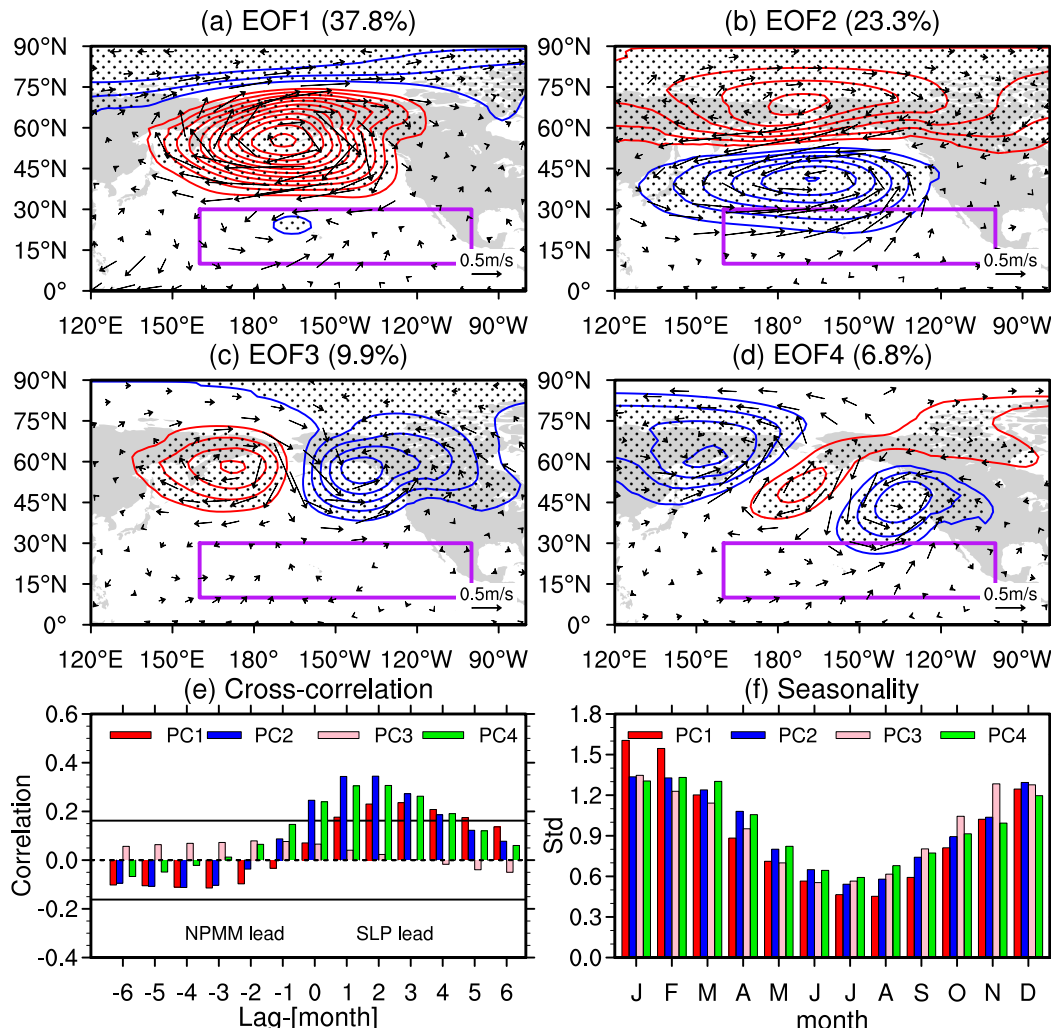


FIG. 5. Leading EOF modes of interannual SLP variability over the North Pacific in the Clim- τ experiment. (a)–(d) Regression maps of 10-yr high-pass filtered SLP [contour interval: 0.4 hPa; solid red (blue) is positive (negative) anomaly; zero contour is omitted] and surface wind (arrows; $m s^{-1}$) anomalies against normalized SLP PCs. The EOF domain is 0° – 70° N, 120° E– 80° W. The purple box is as in Fig. 4, representing the region of NPMM variability. (e) Cross-correlation between SLP PCs and SST EC of interannual NPMM. Black solid lines denote the correlations at 95% confidence interval based on the two-tailed Student's t test. (f) Monthly standard deviation of normalized SLP PCs.

(PC) at month t , which is obtained from an empirical orthogonal function (EOF) analysis of monthly SLP anomalies; t_e denotes the e -folding time scale of 6 months, which is estimated from the decorrelation time scale of the raw PMM SST EC (changing t_e slightly does not affect the result); and the time step dt is 1 month.

Significance tests in this study are all based on a two-tailed Student's t test. The effective degree of freedom is estimated based on the decorrelation time scale of the SST EC of interannual and decadal PMMs (autocorrelation drops to $1/e$), respectively. The number of effective degrees of freedom is approximately the length of SST EC divided by the decorrelation time scale minus 2.

3. Raw PMM

We first investigate the raw PMM by comparing the CTRL simulation with observations and then comparing the Clim- τ simulation with CTRL. Figure 3 shows the regression maps of SST, SLP, and surface wind anomalies against the normalized SST EC of the raw PMMs, along with the seasonality and autocorrelation of the raw PMMs. Overall, the CTRL simulates the NPMM structure, with a southwestward extension of SST warming from the coast of Baja California and trades relaxation, although the extension is displaced more westward and the simulated NPMM magnitude is slightly stronger than that in observations (purple boxes in Figs. 3a and 3b). Additionally, the

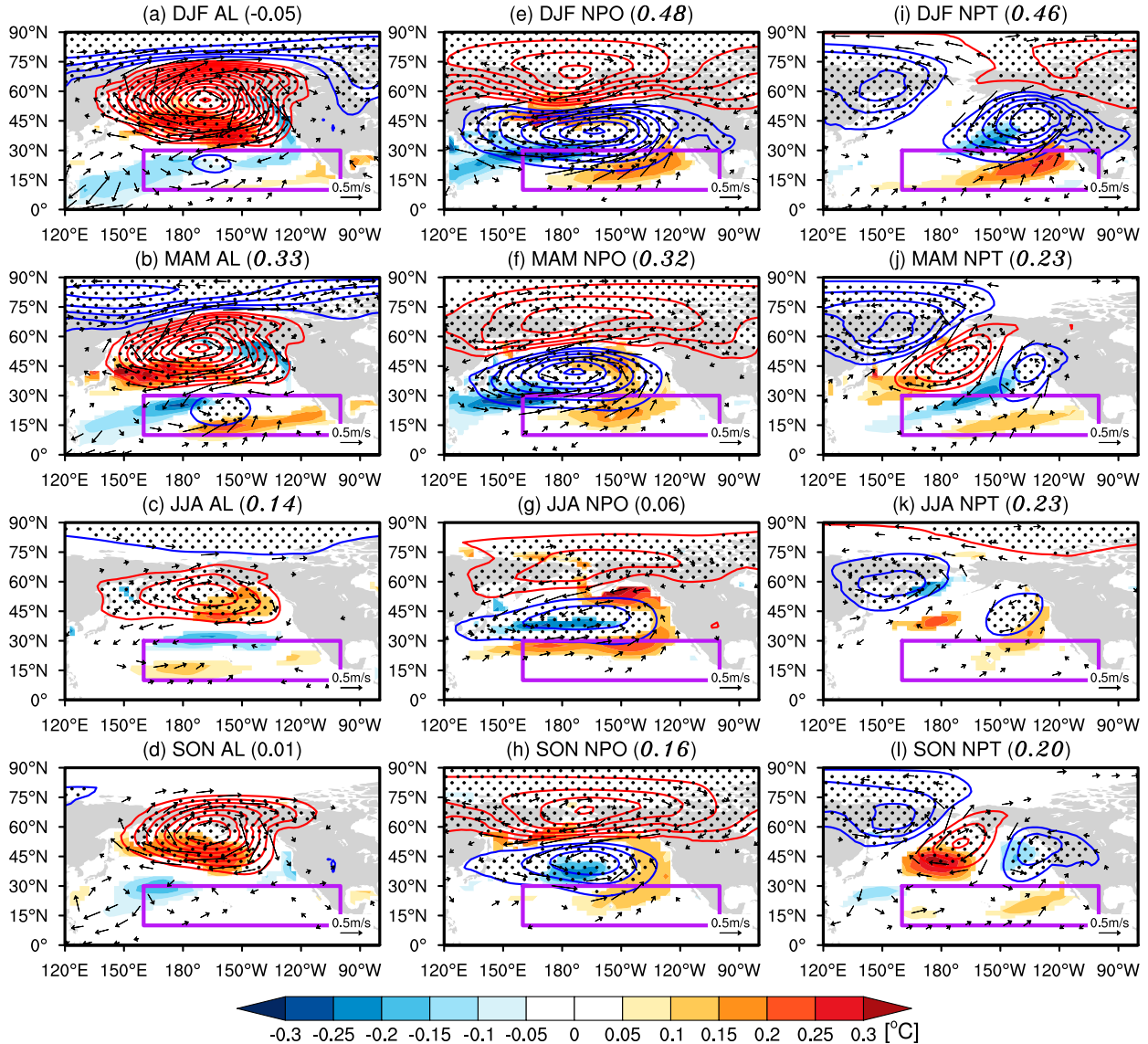


FIG. 6. Seasonality of the interannual (a)–(d) AL, (e)–(h) NPO, and (i)–(l) NPT variability in the Clim- τ experiment. Regression maps of 10-yr high-pass filtered SLP [contour interval: 0.4 hPa; solid red (blue) is positive (negative) anomaly; zero contour is omitted], surface wind ($m s^{-1}$), and SST (shading; $^{\circ}C$) anomalies in different seasons against corresponding normalized seasonal mean SLP PCs. The value in the parentheses in each panel denotes the regression coefficient of seasonal mean SST EC of interannual NPMM variability against corresponding seasonal mean SLP PC. The regression coefficients significant at 95% confidence interval are shown as italic. The purple box in each panel denotes the SVD domain of NPMM variability.

NPMM in the CTRL exhibits more loading over the western equatorial Pacific than that in observations (Figs. 3a,b).

The CTRL also simulates the atmospheric pattern associated with the NPMM over the North Pacific, which resembles the NPO structure (Rogers 1981). Comparing the Clim- τ simulation with the CTRL (Figs. 3b,c), the simulated NPMM and associated ocean-atmosphere variability are mostly confined to the North Pacific, suggesting that the Clim- τ experiment is unique to investigate the NPMM variability without equatorial Pacific influence. The northern lobe of the NPO-like pattern associated with the NPMM in the Clim- τ is

westward displaced slightly compared to the CTRL, causing larger positive SST anomalies southwest of the Bering Strait (Fig. 3c). In addition to the NPMM-related spatial pattern, both the CTRL and Clim- τ capture the seasonality (Fig. 3d) and persistence (Fig. 3e) of the observed NPMM variability. The Clim- τ NPMM autocorrelation decays more quickly than in the CTRL, suggesting that the linear approach to removing ENSO from the CTRL simulation may leave behind statistical artifacts that impact the subtropical North Pacific temporal variability [see discussion in Stuecker (2018)]. In addition, linearly removing ENSO may account for some of the larger differences in the tropical

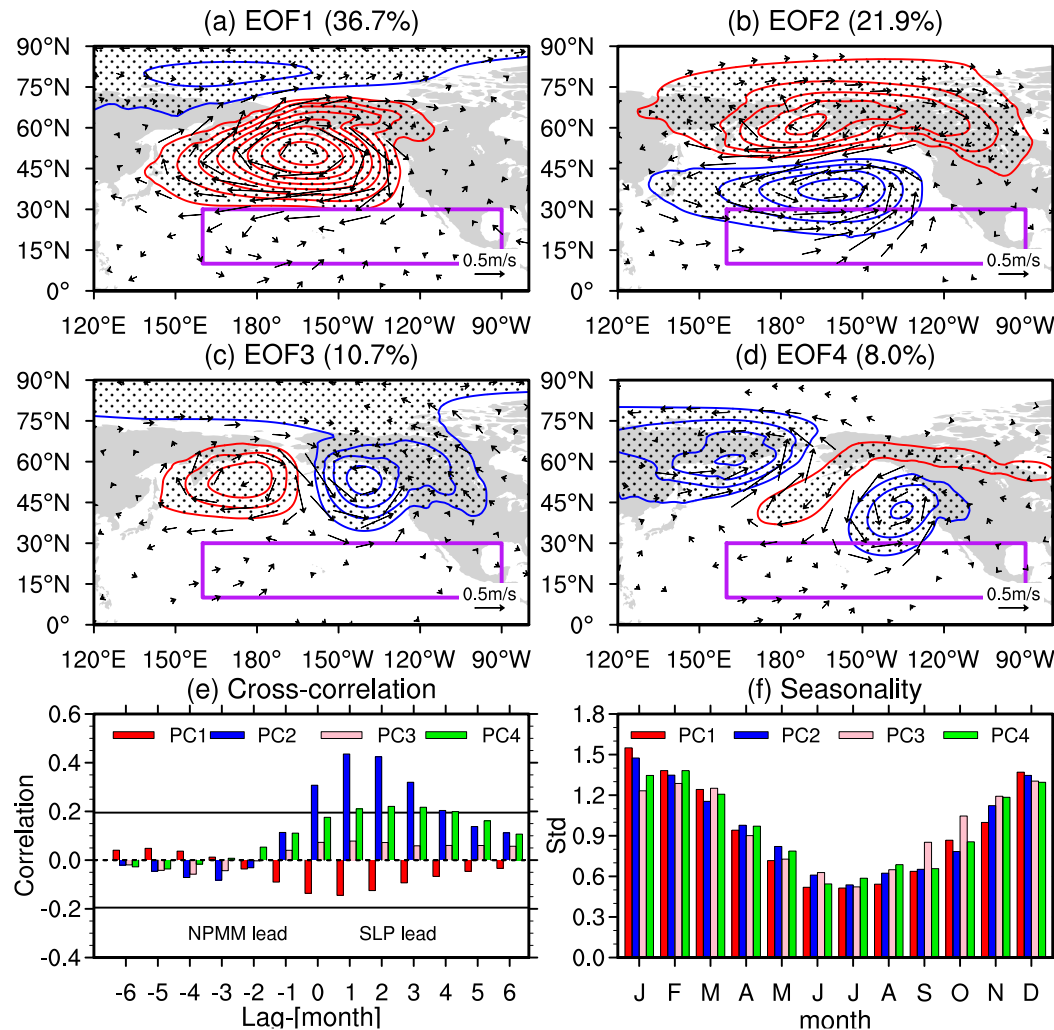


FIG. 7. As in Fig. 5, but for observations.

NPMM spatial pattern between the observation/CTRL and Clim- τ , since lagged and nonlinear ENSO–NPMM interactions are retained in both observations and the CTRL but are effectively removed in Clim- τ . Regardless, the Clim- τ NPMM analysis (Fig. 3c) provides a useful metric to test the null hypothesis that the traditionally defined NPMM index (e.g., Chiang and Vimont 2004) truly captures the leading modes of subtropical coupled climate variability independent of ENSO.

For the raw SPMM, the CTRL captures the observed SPMM structure, with SST warming and trade wind weakening over the subtropical southeastern Pacific (purple boxes in Figs. 3f and 3g), albeit with much stronger amplitude than in observations. The SPMM in the CTRL is strongly associated with an SLP pattern over the entire Southern Hemisphere (Fig. 3g), which is nearly identical to results in a similar mechanically decoupled NCAR CESM experiment (Larson et al. 2018a, their Fig. 11) and to that in Garreaud and Battisti (1999). In contrast, the SPMM in observations is weakly associated with the SLP variability (Fig. 3f). This distinction might be caused by the lack of observations in the South Pacific before the satellite era, or the stronger

simulation of Southern Hemisphere atmospheric variability in the CTRL. In addition, using the wind EC rather than the SST EC of the SPMM variability gives similar results as in You and Furtado (2018). This suggests the sensitivity of selecting different indices to show the SPMM-related SLP pattern. Moreover, the distinction may also be due to the strong interaction between the tropical Pacific and southeastern Pacific variability in observations (e.g., Luo and Yamagata 2001). As a result, removing the effect of tropical Pacific variability on the SPMM will largely reduce the amplitude of both SPMM and associated atmospheric teleconnections. Comparing the Clim- τ simulation with CTRL (Figs. 3g,h), the Clim- τ simulates the SPMM-related variability mostly over the Southern Hemisphere, further highlighting the usefulness of our Clim- τ experiment in studying intrinsic PMM variability. The CTRL well simulates the weak seasonality of the observed SPMM with a slight peak in austral summer, while the Clim- τ shows the opposite with a minor peak in austral winter (Fig. 3i). The SPMM seasonality in our CM2.1 Clim- τ differs from that in the Clim- τ based on the Community Climate System Model

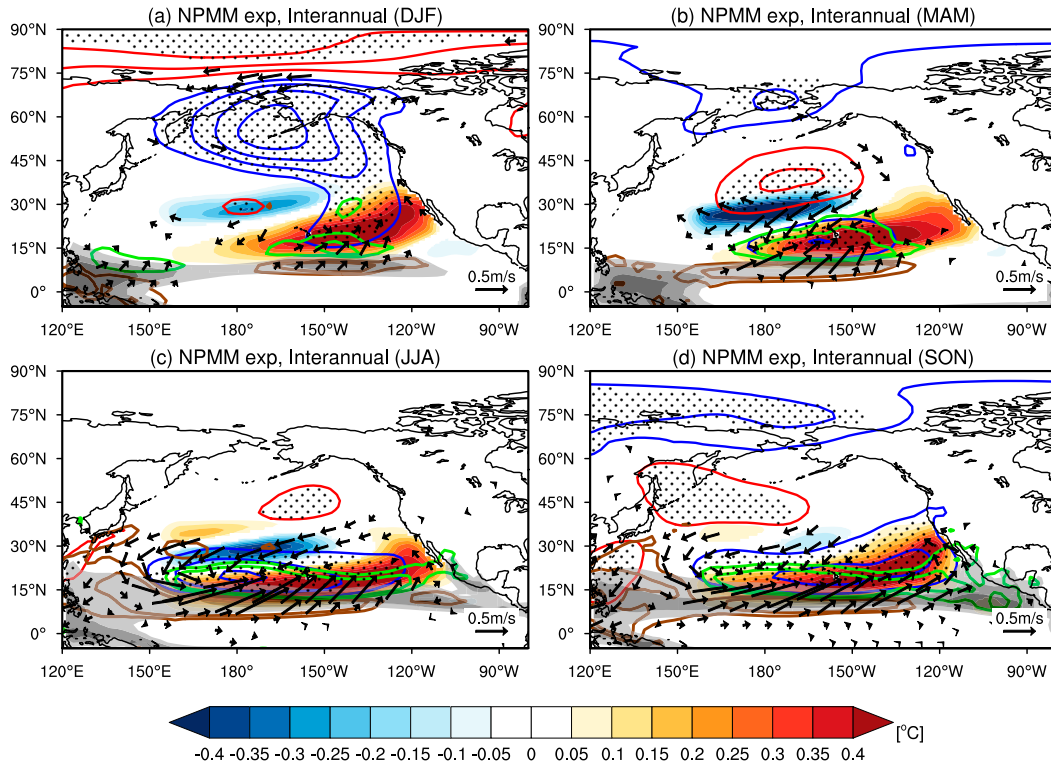


FIG. 8. Atmospheric response to the interannual NPMM in the NPMM experiment: (a) DJF, (b) MAM, (c) JJA, and (d) SON. Patterns are shown as regression maps of 10-yr high-pass filtered SLP [contour interval: 0.2 hPa; solid red (blue) is positive (negative) anomaly; zero contour is omitted], surface wind (arrows; $m s^{-1}$), SST (shading; $^{\circ}C$), and precipitation [contour interval: 0.2 mm day^{-1} ; solid green (brown) is positive (negative)] anomalies against the SST EC of interannual NPMM variability. Climatological precipitation is overlaid as gray shading (only larger than 6 mm day^{-1} are shown, shading interval: 4 mm day^{-1}). The stippling denotes statistically significant regressed SLP at 95% confidence interval.

version 4 (Larson et al. 2018a; see their Fig. 3). This discrepancy might be due to the different seasonality of South Pacific wind variability and/or the seasonal cycle of southeastern Pacific mixed-layer depth, according to the analysis of observed SPMM seasonality from You and Furtado (2018). Future study based on multimodel Clim- τ experiments is needed to deeply investigate the SPMM variability. Finally, to a large extent, the CTRL and Clim- τ capture the persistence of the observed SPMM variability (Fig. 3j). Overall, the simulated spatiotemporal SPMM variability in the Clim- τ can be used for investigating the interannual and decadal SPMM variability, both of which are largely independent of tropical Pacific forcing.

4. NPMM variability

a. Interannual NPMM

We investigate NPMM variability on interannual time scales in observations and in the Clim- τ experiment. Figure 4 shows the regression maps of SST, SLP, and surface wind anomalies against the normalized SST EC of the interannual NPMM. The spatial pattern of interannual NPMM in observations and Clim- τ resemble the respective raw PMMs (comparing Figs. 3a,c and Figs. 4a,b), suggesting that the traditionally

defined NPMM (the raw NPMM) in the literature primarily reflects its interannual variability.

To investigate what dominant atmospheric variability forces interannual NPMM in the Clim- τ experiment, we first extract dominant atmospheric modes by performing EOF analysis to 10-yr high-pass filtered SLP anomalies and then calculate the cross-correlation between SLP PCs and NPMM SST EC in the Clim- τ experiment (Fig. 5). All the EOF modes shown in the following are mutually well separated based on North's rule (North et al. 1982). Figures 5a–d show only features significant at 95% confidence interval based on the two-tailed Student's t test (dotted for SLP).

The first EOF mode is Aleutian low (AL) variability (Fig. 5a), which leads interannual NPMM variability by 2–3 months (Fig. 5e), implying a role in forcing interannual NPMM. Although AL variability primarily features strong SLP anomalies over the Aleutians, westerly anomalies associated with the weak negative SLP anomalies around the Hawaii Islands can weaken trade winds and thereby force NPMM (Fig. 5a). The second EOF mode is NPO variability (Fig. 5b), which leads interannual NPMM variability by 1 month (Fig. 5e), also implying a forcing role. This is consistent with numerous previous studies that relate low pressure anomalies associated with the NPO variability to weakened trade winds and thereby NPMM variability (Fig. 5b;

e.g., Amaya 2019). The third EOF mode is characterized by a zonal dipole pattern along 60°N, which is too far away from the subtropics and cannot influence the strength trade winds or NPMM variability (Figs. 5c,e). The fourth EOF mode exhibits a tripolar structure from northeastern Asia to the northeastern Pacific. Here we term this mode the North Pacific tripole pattern (NPT). Similar to the NPO, the NPT mode also leads NPMM variability by about 1 month, suggestive of its forcing role in the NPMM. Although this mode explains only 6.8% of total interannual SLP variance, the prominent low pressure anomaly over the northeastern Pacific can effectively weaken trade winds and force NPMM (Figs. 5d,e).

To further demonstrate the robustness of the NPT mode, we select a region where SLP variability dominantly forces the interannual NPMM (see Fig. S1a in the online supplemental material) and correlate the SLP index averaged over the region with the NPT PC time series. The result shows that their correlation is statistically significant (Fig. S1b), indicating that although only the center of action over the northeastern Pacific associated with the NPT plays the role in forcing the interannual NPMM, the other two centers of action will covary with this center and collectively force the interannual NPMM. We highlight the necessity of taking the three centers of action as a whole (i.e., the NPT mode) to investigate the relationship with NPMM variability.

As a caveat, the NPT mode obtained by applying EOF analysis to the interannual SLP field may involve the variability forced by the interannual NPMM. To examine whether the NPT mode, like the AL and NPO modes, is an atmospheric internal variability, we analyze an atmosphere-only experiment forced by the global climatological SST and sea ice from the Clim- τ experiment. The result shows that the NPT mode in the atmosphere-only simulation also emerges as the fourth EOF mode (and is also mutually well separated based on North's rule), resembling the one simulated in the Clim- τ in both spatial pattern and magnitude (not shown). Furthermore, the seasonal evolution of the NPT mode in the atmosphere-only simulation is also similar to that in the Clim- τ . These analyses demonstrate that the NPT mode is a mode of atmospheric internal variability.

To further investigate how these atmospheric internal modes (AL, NPO, and NPT) influence interannual NPMM in different seasons, we show their seasonality (Fig. 5f). We then regress seasonal mean SST anomalies against corresponding seasonal mean SLP PCs in December–February (DJF), March–May (MAM), June–July (JJA), and September–November (SON) to examine how the atmospheric modes influence SST variations in the NPMM region (purple box in Fig. 6). The regression patterns are shown significant at 95% confidence interval based on the two-tailed Student's t test. We also compute the regression coefficient of the seasonal mean SST EC of interannual NPMM against corresponding seasonal mean SLP PCs (marked in the title of each panel in Fig. 6).

For the AL variability, although it is strong in DJF (Fig. 6a), the anomalously low pressure around the Hawaiian Islands that effectively weakens trade winds is strong in MAM, resulting in the prominent forcing of interannual NPMM (Fig. 6b). NPO variability is strong in DJF and MAM (Figs. 6e,f). Its southern lobe during these two seasons can affect the strength of trade winds over most of the NPMM domain. In JJA, NPO

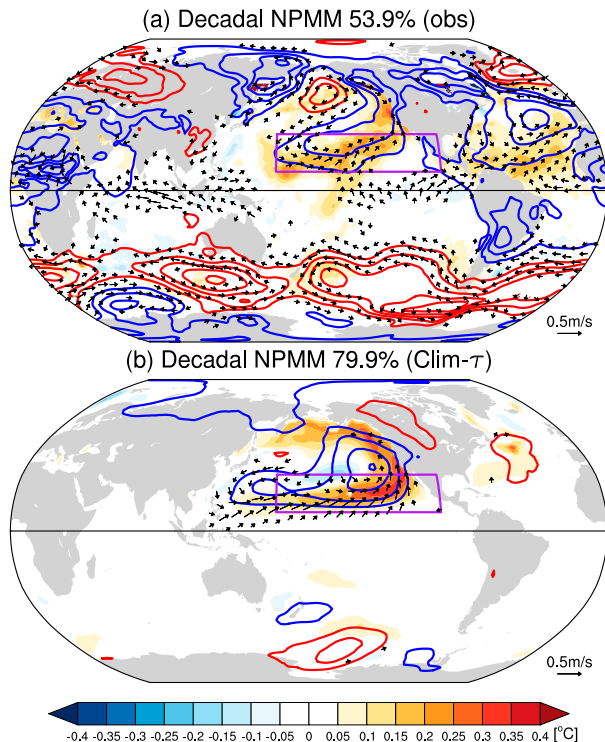


FIG. 9. As in Fig. 4, but for decadal NPMM. Note that contour interval is 0.1 hPa.

variability weakens and its southern lobe only affects the trade winds around $\sim 30^{\circ}$ N, too far to effectively force the interannual NPMM (Fig. 6g). In the subsequent SON, NPO variability strengthens and once again projects onto interannual NPMM (Fig. 6h). Interestingly, although the seasonality of NPT variability resemble that of AL and NPO variability, its impact on the interannual NPMM variability largely persists throughout the year, owing to a persistent anomalous low over the eastern North Pacific, which effectively modulates the strength of trade winds (Figs. 6i–l).

We also examine the atmospheric forcing of the interannual NPMM in observations. To extract the dominant modes of North Pacific atmospheric variability without equatorial Pacific influence, we linearly regress out the CTI-related interannual SLP anomalies for individual calendar months prior to the EOF analysis. EOF1 shows the AL variability (Fig. 7a), which negatively correlates with the interannual NPMM variability (Fig. 7e), in contrast to the result shown in the Clim- τ experiment (Fig. 5e). This negative correlation is because the observed AL center extends farther south than in Clim- τ . Therefore, the associated easterly anomalies in its southern flank strengthen the background trades and then drive negative phase of interannual NPMM via WES feedback. Although the negative correlation is statistically insignificant calculated based on the whole time series, it is significant at 95% confidence interval in MAM ($r = 0.22$).

For the observed NPO variability, it significantly forces the interannual NPMM at 1-month lead (Figs. 7b,e), consistent

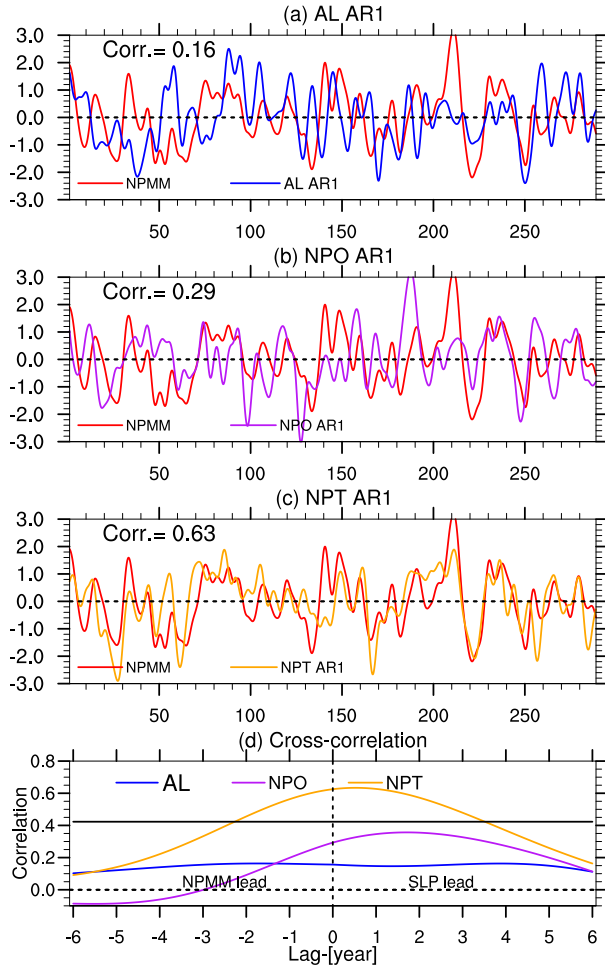


FIG. 10. The 10-yr low-pass filtered reconstructed NPMM time series based on the AR-1 model, as reconstructed by (a) AL variability, (b) NPO variability, and (c) NPT variability. Red lines denote the SST EC of decadal NPMM variability. Correlation between the low-pass filtered reconstructed NPMM time series and the SST EC is marked in each panel. (d) Cross-correlation between the SST EC of decadal NPMM variability and 10-yr low-pass filtered reconstructed NPMM time series forced by AL (blue), NPO (purple), and NPT (yellow) variability based on the AR-1 model. Horizontal solid line denotes the correlation at 95% confidence interval based on the two-tailed Student's *t* test.

with the result shown in the Clim- τ (Fig. 5e). The NPT mode detected in the Clim- τ also exists in observations (and is statistically significant based on North's rule; North et al. 1982; Fig. 7d). Moreover, the observed NPT variability significantly correlates with the interannual NPMM led by 1–3 months (Fig. 7e), suggesting that the NPT plays a role in forcing the interannual NPMM. These observational results are more consistent with the same analysis in CESM1 Clim- τ (not shown) than in CM2.1 Clim- τ . Thus, the distinct result on the role of AL variability in forcing interannual NPMM may be spurious in CM2.1 Clim- τ . Here we conclude that the atmospheric forcing of the interannual NPMM includes NPO and NPT variability.

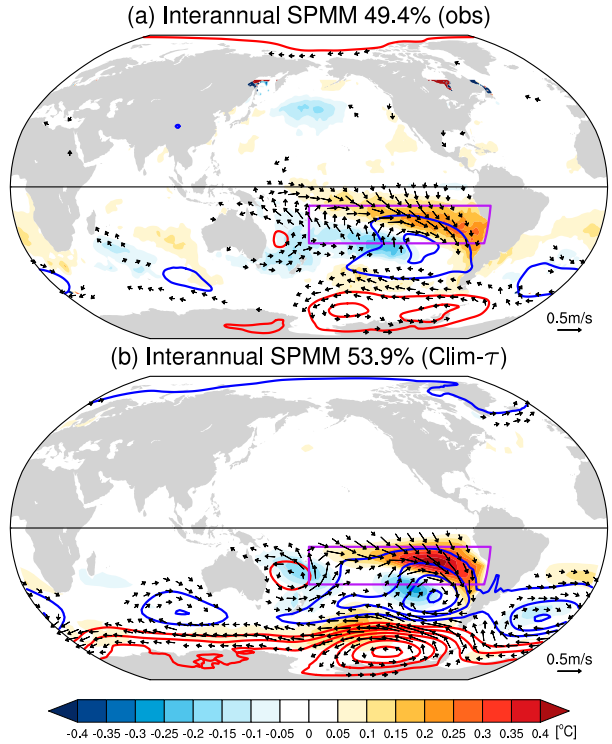


FIG. 11. As in Fig. 4, but for interannual SPMM.

We now examine the atmospheric response to the interannual NPMM in the NPMM experiment. To show the seasonality of the atmospheric response, we regress the seasonal mean atmospheric variability against the corresponding seasonal mean SST EC of interannual NPMM variability (Fig. 8). Patterns are shown significant at 95% confidence interval. The result shows that the atmospheric response to interannual NPMM variability exhibits teleconnection pattern emanating from the subtropical North Pacific to the Arctic. In DJF (Fig. 8a), the atmosphere-forced interannual NPMM encounters the climatological ITCZ at $\sim 150^{\circ}\text{W}$, driving a meridional-dipole pattern of precipitation anomalies. Although the precipitation dipole is weak, a small atmospheric response to the precipitation anomalies may develop quickly and become strong through, for instance, barotropic energy conversion in the exit of subtropical westerly jet during boreal winter (Simmons et al. 1983). The resulting atmospheric response will be an AL-like pattern over the Aleutians (Fig. 8a). This result differs from Amaya et al. (2019), in which they showed that the atmospheric response to the NPMM occurs in late summer and fall when ITCZ is displaced northward. This distinction may be due to the model bias in simulating the latitude of ITCZ in DJF ($\sim 10^{\circ}\text{N}$), which shifts more northward than that in observations ($\sim 5^{\circ}\text{N}$). As a result, the NPMM can influence the meridional displacement of ITCZ and feed back to the atmosphere. Further examination will be needed based on observed ITCZ and NPMM variability.

In MAM (Fig. 8b), as the developed interannual NPMM extends westward, the meridional dipole of precipitation anomaly also moves westward. In JJA (Fig. 8c), with the

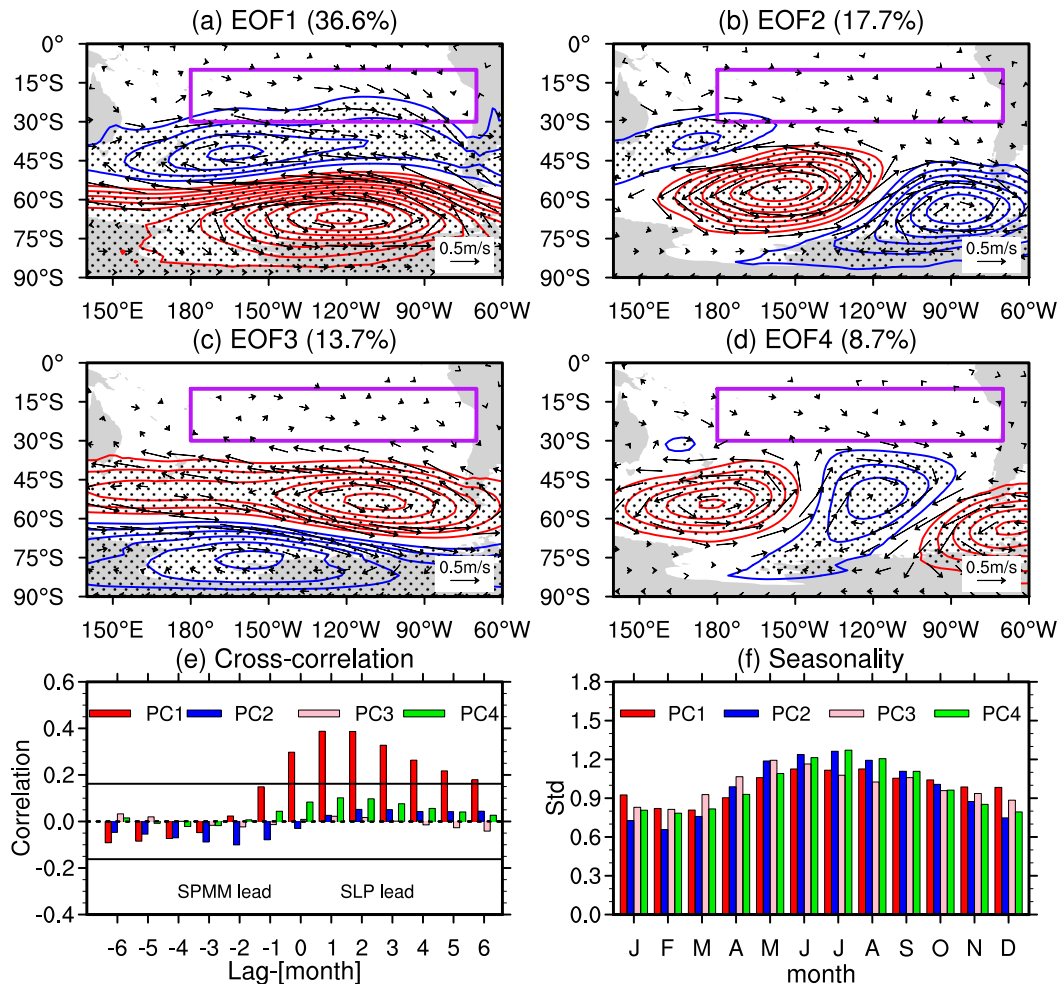


FIG. 12. As in Fig. 5, but for leading EOF modes of interannual SLP variability over the South Pacific in the Clim- τ experiment. The EOF domain is 70°S – 0° , 140°E – 60°W . Purple boxes in (a)–(d) denote the SVD domain of SPMM variability.

farther-westward extension of the NPMM and northward-displaced climatological ITCZ, the precipitation dipole pattern extends zonally along with a broad low pressure anomaly pattern. In SON (Fig. 8d), the zonally broad low pressure anomaly persists and the associated westerly wind anomalies penetrate into the central equatorial Pacific. This atmospheric pattern is reminiscent of the SDC response proposed by Amaya et al. (2019) that takes place in August–October.

We further investigate the upper-tropospheric response to the interannual NPMM variability in the NPMM experiment. The response is not confined to the North Pacific, with teleconnection pattern over the Northern Hemisphere extratropics throughout the year (Fig. S2).

b. Decadal NPMM

We now investigate decadal NPMM variability in observations and the Clim- τ simulation. Figure 9 shows the regression maps of SST, SLP, and surface winds against the normalized SST EC of decadal NPMM variability. The observed decadal

NPMM is associated with variability in both the Northern and Southern Hemispheres (Fig. 9a). The associated SLP anomalies over the Southern Hemisphere extratropics exhibit a meridional seesaw pattern between the mid- and high latitudes. In contrast, the Clim- τ isolates the Pacific-centered characteristics of decadal NPMM variability (Fig. 9b). Similar results are obtained when performing SVD analysis on the model segments with an identical number of time length as in observations (not shown). As a result, the remainder of our analysis will only focus on the Clim- τ experiment.

To explore which dominant mode of atmospheric variability can force the decadal NPMM variability, we compare the 10-yr low-pass filtered reconstructed NPMM index, which is obtained by the AR-1 model (see section 2c for details), with the SST EC of the decadal NPMM variability, and examine their lead-lag relationship (Fig. 10). The AL-forced AR-1 model weakly correlates with the decadal NPMM variability (Figs. 10a,d), suggesting that AL variability cannot effectively force decadal NPMM. In contrast, the correlation between the NPO-forced AR-1 model and decadal

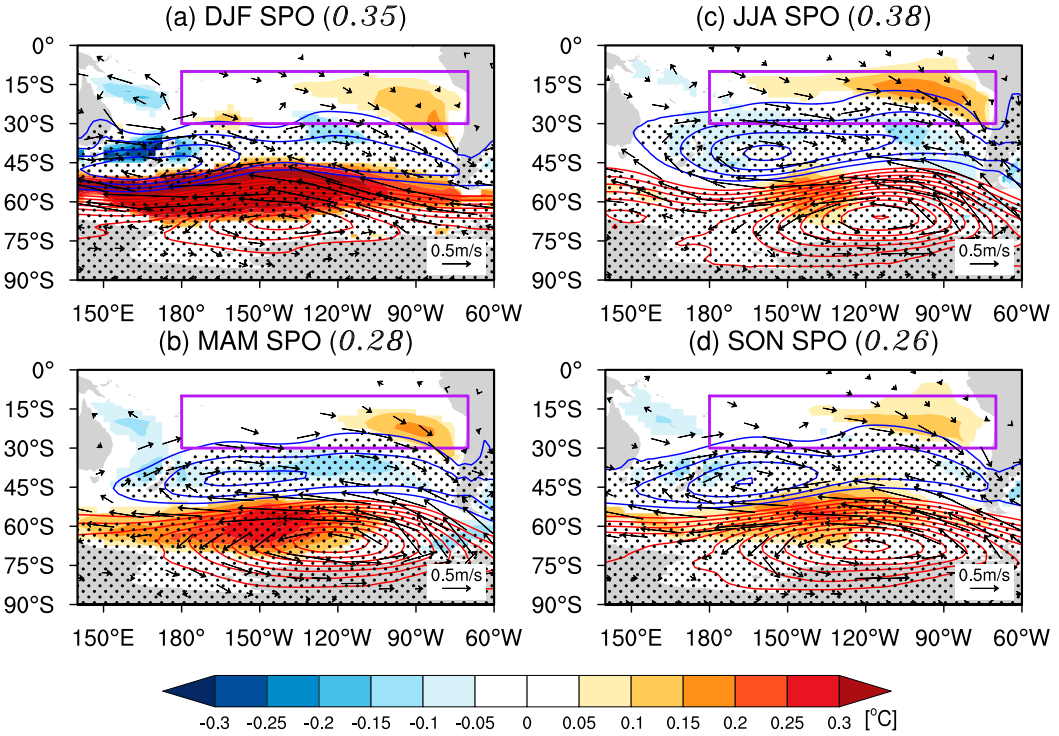


FIG. 13. As in Fig. 6, but for the regression maps of 10-yr high-pass filtered SLP, surface wind, and SST anomalies in different seasons against corresponding normalized seasonal mean SPO PC time series in the Clim- τ experiment. Regression coefficient of seasonal mean SST EC of interannual SPMM against seasonal mean SPO PC time series is marked in each panel.

NPMM variability is slightly larger (Figs. 10b,d). Surprisingly, the NPT-forced AR-1 model best reproduces the decadal NPMM (Figs. 10c,d), suggesting that it is the primary driving role. Similar to the interannual NPMM, the decadal NPMM can also feed back to the atmosphere and excite atmospheric teleconnection in the Northern Hemisphere extratropics (Fig. S3).

5. SPMM variability

a. Interannual SPMM

Next, we investigate SPMM variability on interannual time scales in observations and the Clim- τ . Figure 11 shows the regression maps of SST, SLP, and surface wind anomalies against the normalized SST EC of the interannual SPMM. The interannual SPMM in observations and Clim- τ also resemble the respective raw SPMM, in both structure and magnitude (cf. Figs. 3f,h and Figs. 11a,b), suggesting that the traditionally defined SPMM (the raw SPMM) in the literature also primarily reflects its interannual variability.

To investigate what dominant modes of atmospheric variability over the South Pacific force interannual SPMM, we perform EOF analysis of 10-yr high-pass filtered monthly SLP anomalies over the South Pacific (70°S – 0° , 160°E – 60°W ; results are insensitive to the selected EOF domain) and then compute cross-correlations between SLP PCs and the SST EC of the interannual SPMM variability in the Clim- τ experiment

(Fig. 12). All the EOF modes shown in the following are also mutually well separated based on North's rule (North et al. 1982). The first EOF mode exhibits a meridional dipole pattern, which resembles SPO variability (You and Furtado 2017). This mode can affect the strength of southeastern Pacific trade winds (Fig. 12a) and thereby force SPMM at a 1-month lead (Fig. 12e). Higher-order SLP modes cannot effectively influence trade winds, thus contributing weakly to interannual SPMM variability (Figs. 12b–e). Note that the SPMM-related SLP pattern is not totally identical to the first SLP EOF pattern (cf. Figs. 11b and 12a). This is because the SPMM-related SLP pattern also involves other higher SLP EOF modes, as well as the coupled atmospheric response to the SPMM.

We further decompose the seasonality of SPO variability and quantify its forcing effect by regressing seasonal mean SST anomalies and the SST EC of interannual SPMM variability against normalized the seasonal mean SPO PC time series (Fig. 13). The result suggests that SPO variability can drive interannual SPMM throughout the year, with a slightly stronger forcing effect in JJA, which is largely consistent with its seasonality (Fig. 12f). This result is similar to that of You and Furtado (2018) (see their Fig. 7), which showed that latent heat flux associated with the SPMM variability is strong in boreal summer, indicative of the forcing role of SPO variability.

Next, we investigate the atmospheric response to the interannual SPMM. Figure 14 shows the regressions of seasonal mean atmospheric variability against the corresponding seasonal mean

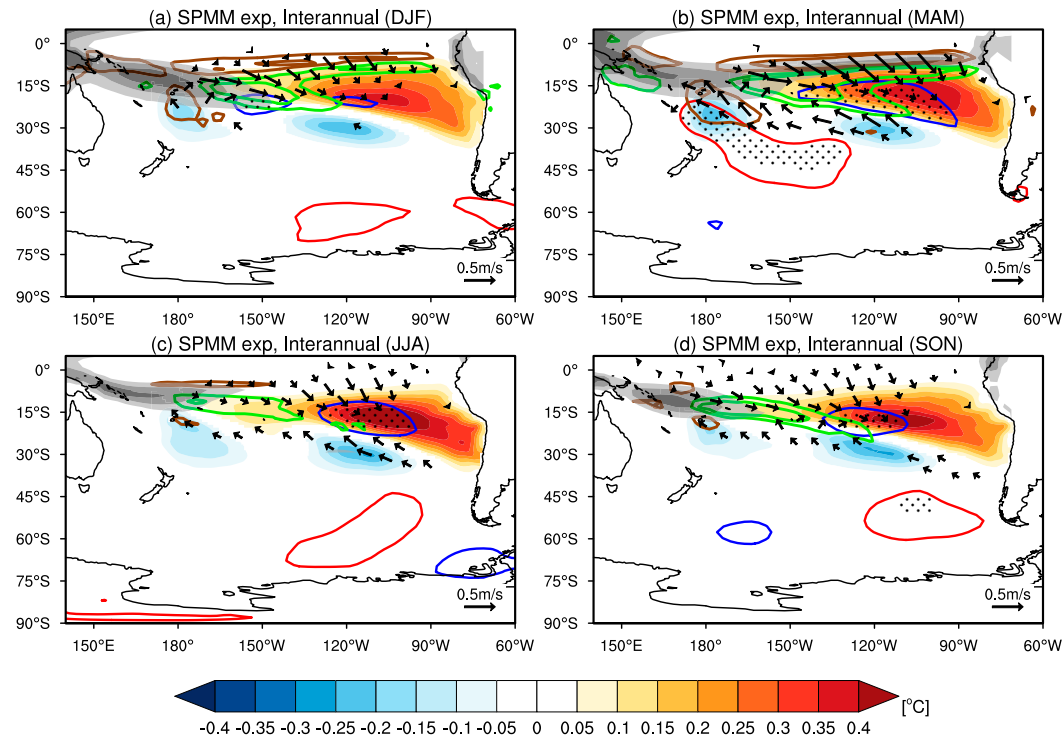


FIG. 14. As in Fig. 8, but for the atmospheric response to the interannual SPMM in the SPMM experiment.

SST EC of interannual SPMM variability in the SPMM experiment. Based on these regressions, the positive phase of interannual SPMM variability can influence the climatological SPCZ, causing southeastward extension along its diagonal throughout the whole year. This finding is similar to that of Min et al. (2017), in which they showed that the SPMM favors an anomalous eastward displacement of the SPCZ (see their Fig. 2d).

We further show that by influencing the mean SPCZ, the interannual SPMM can feed back to the atmosphere, although the feedback amplitude is rather weak compared to that for the interannual NPMM (Fig. 8). In DJF (Fig. 14a), the atmospheric response to the interannual SPMM is rather weak. It is characterized by a convergence of surface wind anomalies $\sim 150^{\circ}\text{W}$, corresponding to a rather weak low pressure center. The anomalous low pressure center becomes stronger in MAM, accompanied by an anomalous high pressure center over the east of New Zealand (Fig. 14b). During DJF and MAM, apart from influencing the SPCZ, the interannual SPMM also impacts ITCZ south of equator. The impact in MAM may be attributed to the model bias of CM2.1 that simulates strong double ITCZ (Wittenberg et al. 2006). In JJA and SON (Figs. 14c,d), the interannual SPMM can also feed back to the atmosphere, with comparable amplitude to those in DJF and MAM. We further show that the atmospheric response to the interannual SPMM is not confined to the South Pacific with large-scale teleconnections in much of the Southern Hemisphere extratropics (Fig. S4).

b. Decadal SPMM

Finally, we investigate decadal SPMM variability in observations and the Clim- τ . The observed decadal SPMM exhibits

SST cooling off the west coast of South America, associated with a seesaw SLP anomaly pattern between the Southern Hemisphere middle and high latitudes (Fig. 15a). In addition, the observed decadal SPMM is also linked to SLP anomalies over the Northern Hemisphere extratropics. The strong linkage of both Northern and Southern Hemispheric circulation anomalies indicates that simultaneously linear-removing EPDV will still retain coherent variability between the Northern and Southern Hemispheres. Moreover, the result of the observed decadal SPMM is not reliable due to the lack of SST measurement in the South Pacific before satellite era. The decadal SPMM in the Clim- τ , in contrast, is simulated largely within Southern Hemisphere extratropics (Fig. 15b). Specifically, it is characterized by SST warming in the southeastern South Pacific, associated with a weakening of southeasterly trade winds. It is also associated with an SPO-like anomaly pattern over the South Pacific. These features related to the decadal SPMM resemble those associated with the interannual SPMM in the Clim- τ (Fig. 11b). To investigate whether the decadal SPMM in the Clim- τ is similar to the interannual variability that is effectively forced by the SPO variability, we reconstruct an SST time series forced by SPO variability based on the AR-1 model. The result shows that the 10-yr low-pass filtered reconstructed time series significantly (at 95% confidence interval) correlates with the SST EC of decadal SPMM (Fig. 15c), suggestive of the role of SPO variability in forcing the decadal SPMM. Similar to the interannual SPMM, decadal SPMM can also feed back to the atmosphere and excite teleconnections over the Southern Hemisphere extratropics through extending/shrinking the climatological

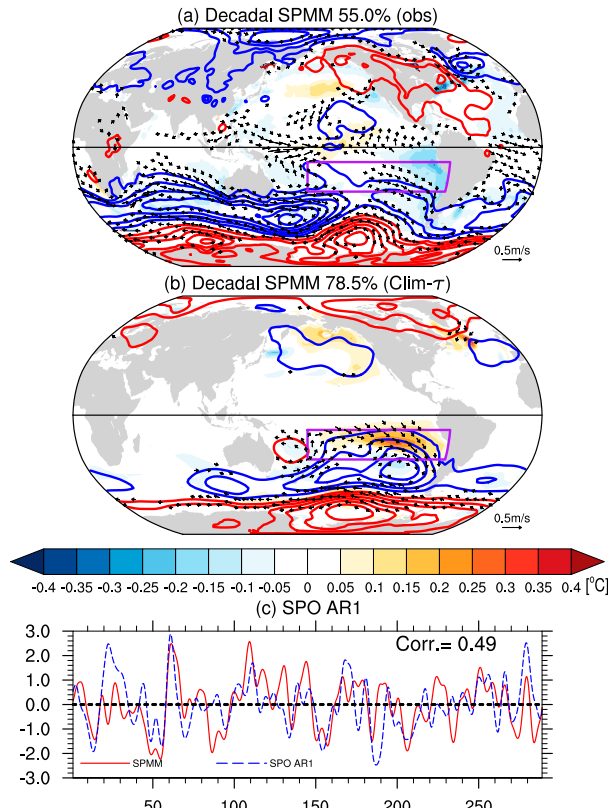


FIG. 15. As in Fig. 4, but for decadal SPMM in (a) observations and (b) the Clim- τ experiment. (c) The 10-yr low-pass filtered reconstructed SPMM time series forced by SPO variability based on the AR-1 model.

SPCZ, but the feedback amplitude is much stronger compared to that for the interannual SPMM (Fig. S5).

6. Summary and discussion

We have investigated the characteristics of both interannual and decadal PMM variability based in a mechanically decoupled model experiment in which climatological wind stress is prescribed over the tropical Pacific. ENSO variability is inhibited in such experiments due to the absence of dynamical air-sea coupling (e.g., Larson and Kirtman 2015). Additionally, TPDV is also markedly damped, due possibly to the dynamical damping effect by the climatological upwelling in the central-eastern equatorial Pacific. This experiment is ideal to investigate essential processes that generate PMM variability, as it cuts off the influence of equatorial Pacific variability on the PMM. Past studies have argued or demonstrated that the NPMM (e.g., Chiang and Vimont 2004; Chang et al. 2007; Ma et al. 2017; Min et al. 2017) and SPMM (e.g., Min et al. 2017; Larson et al. 2018a; You and Furtado 2018; Zhang et al. 2014) can operate in the absence of tropical forcing; this is confirmed in our experiments.

We have explored NPMM and SPMM variability with emphasis on the atmospheric forcing and response processes. For

the NPMM, the atmospheric forcing of its interannual variability differs from the decadal variability. Specifically, interannual NPMM is primarily forced by NPO variability, with a secondary contribution from another atmospheric internal variability, the North Pacific tripole (NPT) mode, while decadal NPMM is primarily forced by the NPT variability. However, the atmospheric response to interannual NPMM variability resembles the response to the decadal NPMM variability in that both can influence the meridional migration of mean ITCZ throughout the whole year. This effect will excite a baroclinic atmospheric response over the subtropical North Pacific and an equivalent barotropic teleconnection pattern over the Northern Hemisphere extratropics. For the SPMM, both interannual and decadal variability are partly forced by SPO variability. Moreover, both can excite atmospheric teleconnections over the Southern Hemisphere extratropics through extending or shrinking the mean SPCZ. Our study proposes a new poleward pathway excited by the NPMM and SPMM variability, in addition to their equatorward influence on tropical Pacific variability (Amaya et al. 2019; Amaya 2019). Further research is needed to examine the robustness of the pathway and its associated climatic effects based on observations.

Although numerous studies have pointed out the role of NPO variability in initiating the NPMM (e.g., Chiang and Vimont 2004; Vimont et al. 2009; Min et al. 2017; Stuecker 2018; Amaya et al. 2019), not much attention is paid to the forcing role of NPT variability. While only the center of action over the northeastern Pacific plays the role in forcing the NPMM, its covariation with the other two centers of action, obtained from the EOF analysis, may mutually initiate the NPMM. In addition, although the NPT mode only explains a small percent of the total variance of SLP variability over the North Pacific, it is more closely tied to decadal NPMM variability than the AL and NPO variability (Fig. 11d), both of which are the contributors to interannual NPMM variability (Fig. 7e). More importantly, the decadal NPMM will release the “reddened” NPT variability to the Northern Hemisphere extratropics, impacting the predictability of Northern Hemisphere extratropical climate. Thus, future studies are needed to investigate the dynamics of NPT variability in observations and modeling experiments.

Acknowledgments. The HadISST v1.1 data are obtained from <https://climatedataguide.ucar.edu/climate-data/sst-data-hadisst-v11>. The ERA-20C data are from <https://apps.ecmwf.int/datasets/data/era20c-moda/levtype=sfc/type=an/>. Y.Z. and X.L. are supported by the National Natural Science Foundation of China (92058203, 41925025) and China’s national key research and development projects (2016YFA0601803). D.J.A. is funded by a Postdoctoral Fellowship with the Cooperative Institute for Research in Environmental Sciences (CIRES) at the University of Colorado Boulder. Y.K. is supported by Japan Society for the Promotion of Science (Grants JP18H01278, JP18H01281, and JP19H05703) and the Integrated Research Program for Advancing Climate Models (JPMXD0717935457). X.W. is supported by the National Key R&D Program of China (2019YFC1510201). A.J.M. is supported by the U.S. NSF (0CE2022868) and NOAA MAPP (NA170AR4310106). This is SOEST contribution 11303 and IPRC publication 1511. We

thank the editor and three anonymous reviewers for providing constructive comments and markedly improving the manuscript.

REFERENCES

- Alexander, M. A., C. Deser, and M. S. Timlin, 1999: The re-emergence of SST anomalies in the North Pacific Ocean. *J. Climate*, **12**, 2419–2433, [https://doi.org/10.1175/1520-0442\(1999\)012<2419:TROSAI>2.0.CO;2](https://doi.org/10.1175/1520-0442(1999)012<2419:TROSAI>2.0.CO;2).
- Amaya, D. J., 2019: The Pacific Meridional Mode and ENSO: A review. *Curr. Climate Change Rep.*, **5**, 296–307, <https://doi.org/10.1007/s40641-019-00142-x>.
- , Y. Kosaka, W. Zhou, Y. Zhang, S.-P. Xie, and A. J. Miller, 2019: The North Pacific pacemaker effect on historical ENSO and its mechanisms. *J. Climate*, **32**, 7643–7661, <https://doi.org/10.1175/JCLI-D-19-0040.1>.
- An, S.-I., and F.-F. Jin, 2004: Nonlinearity and asymmetry of ENSO. *J. Climate*, **17**, 2399–2412, [https://doi.org/10.1175/1520-0442\(2004\)017<2399:NAAOE>2.0.CO;2](https://doi.org/10.1175/1520-0442(2004)017<2399:NAAOE>2.0.CO;2).
- Bellenger, H., E. Guilyardi, J. Leloup, M. Lengaigne, and J. Vialard, 2014: ENSO representation in climate models: From CMIP3 to CMIP5. *Climate Dyn.*, **42**, 1999–2018, <https://doi.org/10.1007/s00382-013-1783-z>.
- Bjerknes, J., 1969: Atmospheric teleconnections from the equatorial Pacific. *Mon. Wea. Rev.*, **97**, 163–172, [https://doi.org/10.1175/1520-0493\(1969\)097<0163:ATFTEP>2.3.CO;2](https://doi.org/10.1175/1520-0493(1969)097<0163:ATFTEP>2.3.CO;2).
- Chang, P., L. Zhang, R. Saravanan, D. J. Vimont, J. C. H. Chiang, L. Ji, H. Seidel, and M. K. Tippett, 2007: Pacific meridional mode and El Niño–Southern Oscillation. *Geophys. Res. Lett.*, **34**, L16608, <https://doi.org/10.1029/2007GL030302>.
- Chiang, J., and D. J. Vimont, 2004: Analogous Pacific and Atlantic meridional modes of tropical atmosphere–ocean variability. *J. Climate*, **17**, 4143–4158, <https://doi.org/10.1175/JCLI4953.1>.
- Delworth, T. L., and Coauthors, 2006: GFDL’s CM2 global coupled climate models. Part I: Formulation and simulation characteristics. *J. Climate*, **19**, 643–674, <https://doi.org/10.1175/JCLI3629.1>.
- Di Lorenzo, E., K. M. Cobb, J. C. Furtado, N. Schneider, B. T. Anderson, A. Bracco, M. A. Alexander, and D. J. Vimont, 2010: Central Pacific El Niño and decadal climate change in the North Pacific. *Nat. Geosci.*, **3**, 762–765, <https://doi.org/10.1038/ngeo984>.
- , G. Liguori, N. Schneider, J. C. Furtado, B. T. Anderson, and M. A. Alexander, 2015: ENSO and meridional modes: A null hypothesis for Pacific climate variability. *Geophys. Res. Lett.*, **42**, 9440–9448, <https://doi.org/10.1002/2015GL066281>.
- Fedorov, A. V., S. Harper, S. Philander, B. Winter, and A. Wittenberg, 2003: How predictable is El Niño? *Bull. Amer. Meteor. Soc.*, **84**, 911–920, <https://doi.org/10.1175/BAMS-84-7-911>.
- Garreaud, R. D., and D. S. Battisti, 1999: Interannual (ENSO) and interdecadal (ENSO-like) variability in the Southern Hemisphere tropospheric circulation. *J. Climate*, **12**, 2113–2123, [https://doi.org/10.1175/1520-0442\(1999\)012<2113:IEAIEL>2.0.CO;2](https://doi.org/10.1175/1520-0442(1999)012<2113:IEAIEL>2.0.CO;2).
- Hu, S., A. V. Fedorov, M. Lengaigne, and E. Guilyardi, 2014: The impact of westerly wind bursts on the diversity and predictability of El Niño events: An ocean energetics perspective. *Geophys. Res. Lett.*, **41**, 4654–4663, <https://doi.org/10.1002/2014GL059573>.
- Hurrell, J. W., and Coauthors, 2013: The Community Earth System Model: A framework for collaborative research. *Bull. Amer. Meteor. Soc.*, **94**, 1339–1360, <https://doi.org/10.1175/BAMS-D-12-00121.1>.
- Joh, Y., and E. Di Lorenzo, 2019: Interactions between Kuroshio Extension and central tropical Pacific lead to preferred decadal-timescale oscillations in Pacific climate. *Sci. Rep.*, **9**, 13558, <https://doi.org/10.1038/s41598-019-49927-y>.
- Larson, S. M., and B. P. Kirtman, 2013: The Pacific meridional mode as a trigger for ENSO in a high-resolution coupled model. *Geophys. Res. Lett.*, **40**, 3189–3194, <https://doi.org/10.1002/grl.50571>.
- , and —, 2014: The Pacific meridional mode as an ENSO precursor and predictor in the North American multimodel ensemble. *J. Climate*, **27**, 7018–7032, <https://doi.org/10.1175/JCLI-D-14-00055.1>.
- , and —, 2015: Revisiting ENSO coupled instability theory and SST error growth in a fully coupled model. *J. Climate*, **28**, 4724–4742, <https://doi.org/10.1175/JCLI-D-14-00731.1>.
- , K. V. Pégion, and B. P. Kirtman, 2018a: The South Pacific meridional mode as a thermally driven source of ENSO amplitude modulation and uncertainty. *J. Climate*, **31**, 5127–5145, <https://doi.org/10.1175/JCLI-D-17-0722.1>.
- , D. J. Vimont, A. C. Clement, and B. P. Kirtman, 2018b: How momentum coupling affects SST variance and large-scale Pacific climate variability in CESM. *J. Climate*, **31**, 2927–2944, <https://doi.org/10.1175/JCLI-D-17-0645.1>.
- Liguori, G., and E. Di Lorenzo, 2019: Separating the North and South Pacific meridional modes contributions to ENSO and tropical decadal variability. *Geophys. Res. Lett.*, **46**, 906–915, <https://doi.org/10.1029/2018GL080320>.
- Liu, Z., and E. Di Lorenzo, 2018: Mechanisms and predictability of Pacific decadal variability. *Curr. Climate Change Rep.*, **4**, 128–144, <https://doi.org/10.1007/s40641-018-0090-5>.
- Lu, F., Z. Liu, Y. Liu, S. Zhang, and R. Jacob, 2017: Understanding the control of extratropical atmospheric variability on ENSO using a coupled data assimilation approach. *Climate Dyn.*, **48**, 3139–3160, <https://doi.org/10.1007/s00382-016-3256-7>.
- Luo, J., and T. Yamagata, 2001: Long-term El Niño–Southern Oscillation (ENSO)-like variation with special emphasis on the South Pacific. *J. Geophys. Res.*, **106**, 22 211–22 227, <https://doi.org/10.1029/2000JC000471>.
- Ma, J., S. P. Xie, and H. Xu, 2017: Contributions of the North Pacific meridional mode to ensemble spread of ENSO prediction. *J. Climate*, **30**, 9167–9181, <https://doi.org/10.1175/JCLI-D-17-0182.1>.
- McGregor, S., A. Timmermann, N. Schneider, M. F. Stuecker, and M. H. England, 2012: The effect of the South Pacific convergence zone on the termination of El Niño events and the meridional asymmetry of ENSO. *J. Climate*, **25**, 5566–5586, <https://doi.org/10.1175/JCLI-D-11-0032.1>.
- McPhaden, M. J., 2003: Tropical Pacific Ocean heat content variations and ENSO persistence barriers. *Geophys. Res. Lett.*, **30**, 1480, <https://doi.org/10.1029/2003GL016872>.
- Min, Q., J. Su, and R. Zhang, 2017: Impact of the South and North Pacific meridional modes on the El Niño–Southern Oscillation: Observational analysis and comparison. *J. Climate*, **30**, 1705–1720, <https://doi.org/10.1175/JCLI-D-16-0063.1>.
- North, G. R., T. L. Bell, R. F. Cahalan, and F. J. Moeng, 1982: Sampling errors in the estimation of empirical orthogonal functions. *Mon. Wea. Rev.*, **110**, 699–706, [https://doi.org/10.1175/1520-0493\(1982\)110<0699:SEITEO>2.0.CO;2](https://doi.org/10.1175/1520-0493(1982)110<0699:SEITEO>2.0.CO;2).
- Okumura, Y., 2013: Origins of tropical Pacific decadal variability: Role of stochastic atmospheric forcing from the South Pacific. *J. Climate*, **26**, 9791–9796, <https://doi.org/10.1175/JCLI-D-13-00448.1>.
- Pégion, K., C. M. Selman, S. Larson, J. C. Furtado, and E. J. Becker, 2020: The impact of the extratropics on ENSO diversity and predictability. *Climate Dyn.*, **54**, 4469–4484, <https://doi.org/10.1007/s00382-020-05232-3>.

- Poli, P., and Coauthors, 2016: ERA-20C: An atmospheric reanalysis of the twentieth century. *J. Climate*, **29**, 4083–4097, <https://doi.org/10.1175/JCLI-D-15-0556.1>.
- Rasmusson, E. M., and T. H. Carpenter, 1982: Variations in tropical sea surface temperature and surface wind fields associated with the Southern Oscillation/El Niño. *Mon. Wea. Rev.*, **110**, 354–384, [https://doi.org/10.1175/1520-0493\(1982\)110<0354:VITSST>2.0.CO;2](https://doi.org/10.1175/1520-0493(1982)110<0354:VITSST>2.0.CO;2).
- Rayner, N. A., D. E. Parker, E. B. Horton, C. K. Folland, L. V. Alexander, D. P. Rowell, E. C. Kent, and A. Kaplan, 2003: Global analyses of sea surface temperature, sea ice, and night marine air temperature since the late nineteenth century. *J. Geophys. Res.*, **108**, 4407, <https://doi.org/10.1029/2002JD002670>.
- Rogers, J. C., 1981: The North Pacific Oscillation. *J. Climatol.*, **1**, 39–57, <https://doi.org/10.1002/joc.3370010106>.
- Simmons, A. J., J. M. Wallace, and G. Branstator, 1983: Barotropic wave propagation and instability, and atmospheric teleconnection patterns. *J. Atmos. Sci.*, **40**, 1363–1392, [https://doi.org/10.1175/1520-0469\(1983\)040<1363:BWPAIA>2.0.CO;2](https://doi.org/10.1175/1520-0469(1983)040<1363:BWPAIA>2.0.CO;2).
- Slingo, J. M., D. P. Rowell, K. R. Sperber, and F. Nortley, 1999: On the predictability of the interannual behavior of the Madden-Julian oscillation and its relationship with El Niño. *Quart. J. Roy. Meteor. Soc.*, **125**, 583–609, <https://doi.org/10.1002/qj.49712555411>.
- Stuecker, M. F., 2018: Revisiting the Pacific meridional mode. *Sci. Rep.*, **8**, 3216, <https://doi.org/10.1038/s41598-018-21537-0>.
- Thomas, E. E., and D. J. Vimont, 2016: Modeling the mechanisms of linear and nonlinear ENSO responses to the Pacific meridional mode. *J. Climate*, **29**, 8745–8761, <https://doi.org/10.1175/JCLI-D-16-0090.1>.
- Timmermann, A., and Coauthors, 2018: El Niño–Southern Oscillation complexity. *Nature*, **559**, 535–545, <https://doi.org/10.1038/s41586-018-0252-6>.
- Vimont, D. J., J. M. Wallace, and D. S. Battisti, 2003: The seasonal footprinting mechanism in the Pacific: Implications for ENSO. *J. Climate*, **16**, 2668–2675, [https://doi.org/10.1175/1520-0442\(2003\)016<2668:TSFMIT>2.0.CO;2](https://doi.org/10.1175/1520-0442(2003)016<2668:TSFMIT>2.0.CO;2).
- , M. A. Alexander, and A. Fontaine, 2009: Midlatitude excitation of tropical variability in the Pacific: The role of thermodynamic coupling and seasonality. *J. Climate*, **22**, 518–534, <https://doi.org/10.1175/2008JCLI2220.1>.
- Wittenberg, A. T., A. Rosati, N. C. Lau, and J. J. Ploshay, 2006: GFDL's CM2 global coupled climate models. Part III: Tropical Pacific climate and ENSO. *J. Climate*, **19**, 698–722, <https://doi.org/10.1175/JCLI3631.1>.
- Wu, S., L. Wu, Q. Liu, and S.-P. Xie, 2010: Development processes of the tropical Pacific meridional mode. *Adv. Atmos. Sci.*, **27**, 95–99, <https://doi.org/10.1007/s00376-009-8067-x>.
- Wyrtki, K., 1975: El Niño—The dynamic response of the equatorial Pacific Ocean to atmospheric forcing. *J. Phys. Oceanogr.*, **5**, 572–584, [https://doi.org/10.1175/1520-0485\(1975\)005<0572:ENTDRO>2.0.CO;2](https://doi.org/10.1175/1520-0485(1975)005<0572:ENTDRO>2.0.CO;2).
- Xie, S.-P., and S. G. H. Philander, 1994: A coupled ocean–atmosphere model of relevance to the ITCZ in the eastern Pacific. *Tellus*, **46A**, 340–350, <https://doi.org/10.3402/tellusa.v46i4.15484>.
- You, Y., and J. C. Furtado, 2017: The role of South Pacific atmospheric variability in the development of different types of ENSO. *Geophys. Res. Lett.*, **44**, 7438–7446, <https://doi.org/10.1002/2017GL073475>.
- , and —, 2018: The South Pacific meridional mode and its role in tropical Pacific climate variability. *J. Climate*, **31**, 10 141–10 163, <https://doi.org/10.1175/JCLI-D-17-0860.1>.
- Zebiak, S. E., and M. A. Cane, 1987: A model El Niño–Southern Oscillation. *Mon. Wea. Rev.*, **115**, 2262–2278, [https://doi.org/10.1175/1520-0493\(1987\)115<2262:AMENO>2.0.CO;2](https://doi.org/10.1175/1520-0493(1987)115<2262:AMENO>2.0.CO;2).
- Zhang, H., A. Clement, and P. N. DiNezio, 2014: The South Pacific meridional mode: A mechanism for ENSO-like variability. *J. Climate*, **27**, 769–783, <https://doi.org/10.1175/JCLI-D-13-00082.1>.
- Zhao, Y., and E. Di Lorenzo, 2020: The impacts of extra-tropical ENSO Precursors on tropical Pacific decadal-scale variability. *Sci. Rep.*, **10**, 3031, <https://doi.org/10.1038/s41598-020-59253-3>.